Climate-related signals in the GV7-C ice core from East Antarctica for 1782–2013 CE: Potential relevance to climate and teleconnections between tropics and Antarctica

Yalalt Nyamgerel[1,2], Yeongcheol Han[3], Soon Do Hur[3], Hyemi Kim[1], Songyi Kim[1,3], Jangil Moon[3], Barbara Stenni[4], Jeonghoon Lee[1]*

[1]Department of Science Education, Ewha Womans University, Seoul 120-750, Republic of Korea
[2]Institute of Chemistry and Chemical Technology of Mongolian Academy of Sciences, Ulaanbaatar 13260, Mongolia
[3]Division of Glacier and Earth Sciences, Korea Polar Research Institute, Incheon 21990, Republic of Korea
[4]Department of Environmental Sciences, Informatics and Statistics, Ca' Foscari University, Venice 30123, Italy

Correspondence to: Jeonghoon Lee (jeonghoon.d.lee@gmail.com)

Abstract. Polar ice cores provide valuable archives of past climate variability, but interpreting these records in coastal East Antarctica remains challenging because multiple meteorological processes can influence the signals preserved in ice core. Here we investigate climate-related signals in the GV7-C ice core from East Antarctica (1782–2013 CE) using annual records of water isotopes ($\delta^{18}O$ and *d*-excess) and snow accumulation, by comparing them with large-scale climate indices and reanalysis-based climate data. Snow accumulation shows strong interannual variability, suggesting multiple and potentially competing controls, and is weakly linked to sea-surface temperature variability over the Indian Ocean Sector (1957–2013 CE). $\delta^{18}O$ exhibits relatively detectable relationships to Pacific-sector variability for 1957–2013 CE, whereas *d*-excess shows clearer relationships with sea-surface temperature variability in the Indian Ocean sector. Over the longer period (1872–2013 CE), $\delta^{18}O$ correlations generally weaken, implying time-varying controls, while *d*-excess retains persistent relationships, highlighting its utility for tracking moisture-source conditions. Overall, the GV7-C record suggests potential teleconnections between Antarctic coastal climate and tropical ocean variability.

1 Introduction

Climate variability over Antarctica and the surrounding Southern Ocean is crucial for the global climate system (Mayewski et al., 2009; Fretwell et al., 2013; Rintoul et al., 2018). However, the Antarctic climate system is complex (Masson-Delmotte et al., 2008), with large variations in near-surface air temperature (Nicolas and Bromwich, 2014; Constable et al., 2022) and surface mass balance (Dalaiden et al., 2020a), sparse observational coverage, and high natural variability (Kim et al., 2020; Klein et al., 2019), with particularly pronounced variability in coastal regions (Tuohy et al., 2015; Stenni et al., 2017; Goursaud et al., 2019). Ice-core records provide a means to reconstruct past climatic and environmental conditions. Stable water isotopes ($\delta^{18}O$ and δD) in ice cores can reflect relative changes in temperature (Jouzel et al., 1997; Markle and Steig, 2022), sea ice extent (SIE), and atmospheric circulation (Thomas and Abram, 2016). Atmospheric circulation patterns have been reported as important factors influencing isotopic signals in Antarctic ice cores (Bertler et al., 2004; Kino et al., 2021; Leroy-Dos Santos et al., 2023). The relationships between isotopes, temperature, and surface mass balance depend on the relative contributions of large-scale dynamical and thermodynamic processes (Oerter et al., 2000; Medley et al., 2018; Goursaud et al., 2019; Dalaiden et al., 2020b). Moreover, the influence of the Southern Annular Mode (SAM), which describes shifts in the Southern Hemisphere westerlies (Hall and Visbeck, 2002; Fogt et al., 2012), has been evidenced in $\delta^{18}O$ and surface mass balance records from coastal Antarctic ice cores (Schlosser et al., 2014; Servettaz et al., 2020). The second-order parameter *d*-excess (*d*-excess = $\delta D - 8 \times \delta^{18}O$), which is sensitive to relative humidity and sea-surface temperature (SST) at the moisture source (Jouzel et al., 1982; Delmotte et al., 2000; Uemura et al., 2008), has been used to infer source-region conditions (Stenni et al., 2001; Sodemann and Stohl, 2009). Snow accumulation (SA) rates estimated from ice cores can also respond to changes in moisture availability and circulation, and may increase in warmer climates (Frieler et al., 2015; Palerme et al., 2017) and under low sea-ice conditions in coastal regions (Nyamgerel et al., 2020), although the strength and mechanisms of these relationships can be site dependent (Dalaiden et al., 2020a).

In recent decades, SAM variability has exerted a strong influence on Southern Hemisphere climate (Russell and McGregor, 2010), affecting the spatial variability of temperature, precipitation, and sea ice across Antarctica (Nicolas and Bromwich, 2014; Purich et al., 2016; Kim et al., 2020), while also modulating regional atmospheric circulation patterns that can amplify or dampen local climate responses. Antarctic surface mass balance is also linked to the El Niño–Southern Oscillation (ENSO) (Kim et al., 2020), with its influence varying depending on seasonal phasing and interaction with other climate modes such as SAM. Teleconnections between Antarctic and tropical climate variability have been reported in ice-core records (Yuan, 2004; Schneider and Steig, 2008), but their expression can be complex, non-stationary, and dependent on timescale and the concurrent state of multiple climate modes (e.g., ENSO and SAM), which can limit detectability in ice-core records (Divine et al., 2009; Turner et al., 2009).

There remains considerable ambiguity regarding the geographical extent and temporal stability of climate signals derived from Antarctic ice cores (Stenni et al., 2017). Differences in spatial and temporal variability indicate the need for

additional regionally focused records, particularly in coastal East Antarctica (Vance et al., 2016; Goursaud et al., 2017). The GV7-C ice core site, characterized by relatively high snow accumulation, provides a well-dated and high-resolution record (Caiazzo et al., 2017; Nardin et al., 2021). Here we explore climate-related signals in annual GV7-C records of $\delta^{18}O$, *d*-excess, and SA for 1782–2013 CE. The record is compared with climate variables at annual and seasonal timescales, recognizing that ice-core isotopic signals integrate source conditions, transport pathways, and rainout processes (Jackson et al., 2023). Particular attention is given to potential remote influences from ENSO and SAM, as suggested by a previous study for 1979–2012 CE (Khan, 2019). This study provides additional insights from the GV7-C ice core into potential teleconnections between the tropics and coastal East Antarctica.

2 Materials and methods

2.1 Study area

During the 2013/14 Antarctic summer season, a collaborative Italian/Korean expedition drilled several firn–ice cores at the GV7 drilling site (70°41′ S, 158°52′ E; 1950 m a.s.l.) on the Oates Coast, East Antarctica (Fig. 1). Six shallow firn cores (5–50 m) and intermediate firn and ice cores (78–250 m) were recovered; the 78 m core (GV7-C) is used in this study. The site is approximately 95 km from the nearest coastline of the Southern Ocean, while the distance to open water varies seasonally with sea-ice conditions. Ice velocity at this location is very low (< 0.3 m yr^{-1}) and the 10 m firn temperature is –31.8 °C (Frezzotti et al., 2007). Snow accumulation is relatively high and post-depositional effects are limited due to the low intensity of katabatic winds along the ice divide (Becagli et al., 2004; Frezzotti et al., 2007; Magand et al., 2004). Based on 2007–2012 back-trajectory and precipitation-source analyses (Caiazzo et al., 2017), the dominant air-mass influence varies seasonally (e.g., enhanced western Pacific influence in autumn to winter and Ross Sea influence in spring), while overall trajectory statistics show frequent pathways from the Indian Ocean sector (32%) and the Antarctic Plateau (29%), with smaller contributions from the Ross Sea (21%) and western Pacific (19%). The western Pacific and Indian Ocean sectors accounted for ~59% (147 mm) and ~28% (69 mm) of total precipitation (250 mm), respectively (Caiazzo et al., 2017). Snow accumulation at GV7 is estimated to be higher in austral summer and autumn, with a secondary winter maximum associated with pathways from the Antarctic Plateau and Indian Ocean sectors (Caiazzo et al., 2017).

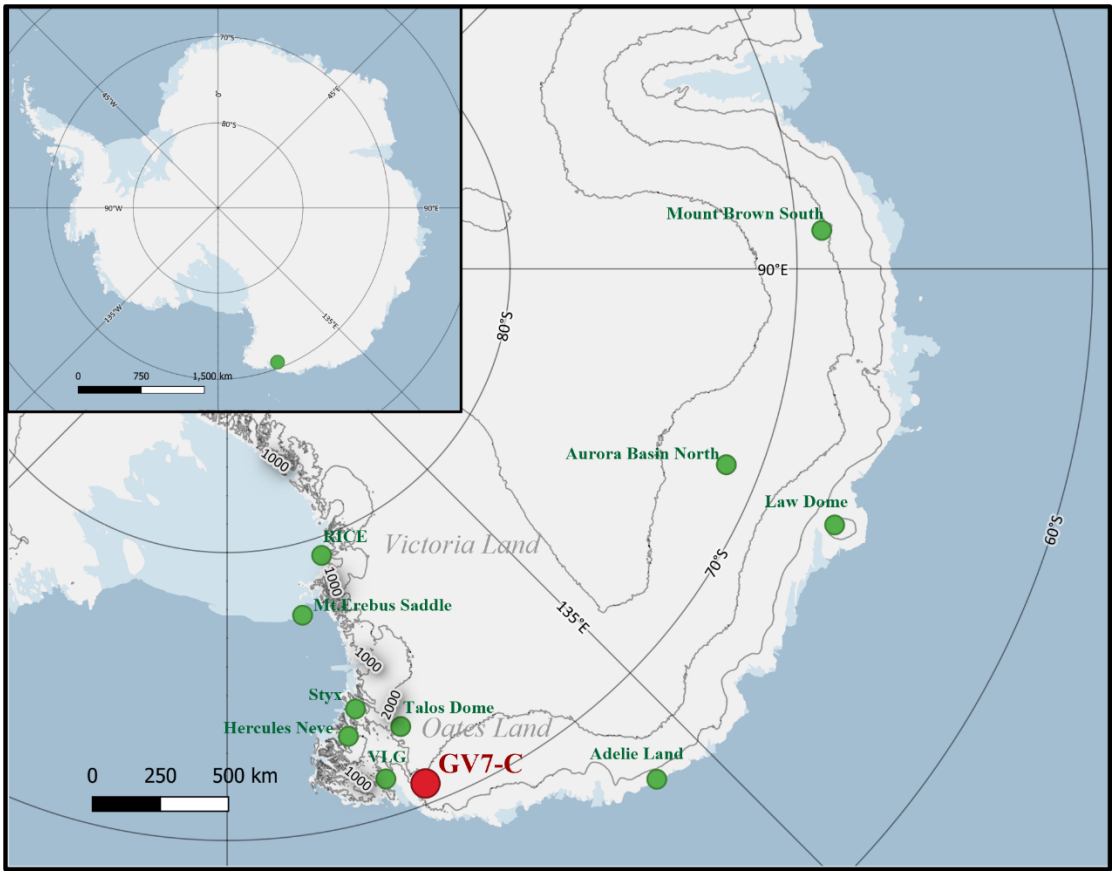


Figure 1. Location of the GV7-C ice core (red) and other ice core sites (green) in East Antarctica. RAMP2 elevation contours (1000 m) are shown (Liu et al., 2015). The map was generated using QGIS software with Quantarctica3 project data (Matsuoka et al., 2021).

2.2 Ice core data

The 78 m long GV7-C ice core was collected in 107 runs and has an average diameter of ~0.08 m. Density was estimated from the mass and dimensions of subsections. Core sections were kept frozen and transported to Korea. In the cold room at the Korea Polar Research Institute (KOPRI), the core was cut to an average sample length of 0.04 m (range 0.03–0.07 m) for stable water isotope analysis ($\delta^{18}O$ and δD). A total of 1880 samples were analyzed using cavity ring-down spectrometers (L2130-I and L2140-i, Picarro Inc., USA) at KOPRI. Annual layers were identified from the seasonal summer maximum $\delta^{18}O$ peaks, and sample ages were assigned by linear interpolation between two consecutive peaks. The GV7-C ice-core record covers 1782–2013 CE. The seasonal $\delta^{18}O$ pattern has been reported previously (Caiazzo et al., 2017; Nardin et al., 2021). Annual layer counting was further constrained using electrical conductivity measurements with a Portable ECM unit (Icefield Instruments Inc., Canada). Conductivity peaks associated with Pinatubo (1991 CE), Agung (1963 CE), Tarawera (1886 CE), Krakatau (1883 CE), and Tambora (1815 CE) were used as additional time markers. Annual mean $\delta^{18}O$, δD, and *d*-excess were calculated as the arithmetic mean of all isotope measurements assigned to each annual layer (i.e., between two successive summer maxima). The annual mean snow accumulation (SA) rate was estimated by multiplying the annual-layer thickness by the measured density of the corresponding core sections and is reported in millimeters water equivalent per year (mm w.e. yr^{-1}). The *d*-excess ($d\text{-excess} = \delta D - 8 \times \delta^{18}O$) was calculated from $\delta^{18}O$ and δD. Data points per year ranged from 3 to 21 (average 8); some years therefore do not fully resolve all seasons and seasonal means are not consistently available. Accordingly, annual means of $\delta^{18}O$, *d*-excess, and SA are used in the correlation analyses.

2.3 Climate data and analysis

The $\delta^{18}O$ ($\delta^{18}O$ is preferred because it is highly correlated with δD; r = 0.99), *d*-excess, and SA from the GV7-C ice core were used in the correlation analysis. Two time periods (1957–2013 CE and 1872–2013 CE) were selected for correlation analyses between GV7-C records and climate variables based on data availability (e.g., SAM indices) and to ensure adequate sample size. The annual means of the ice core records derived from multiple intra-annual samples (3–21 data points per year; average 8) were used in the correlation analysis, which reduces the influence of seasonal extreme values. Because isotopic composition recorded in an annual layer reflects integrated snowfall through the year, GV7-C records represent the combined influence of seasonal processes. For the climate data, we therefore examined at both annual (January–December) and seasonal (DJF, MAM, JJA, SON) scales to assess potential relationships. Although some seasonal differences were observed, overall patterns and physical interpretations were consistent when annual means were used; therefore, annual values are presented to represent the net integrated climate signal preserved in the ice core. Correlation analyses were conducted on original and linearly detrended time series (annual and three-year running averages) of the ice core and climate data, and the results are described in Sections 3.3.1 – 3.3.2. The correlation analysis on the smoothed time series were conducted to reduce stratigraphic noise, and at least three-year averaging has been suggested for obtaining a significant climatic signal from the GV7 site (e.g., Frezzotti et al., 2007; Khan et al., 2021; Schlosser and Oerter, 2002). Pearson correlation coefficients were calculated and their significance was assessed using a two-tailed Student's t-test with corresponding *p*-values. Although, the ice core and climate data were annually averaged and linear trends were removed, the effects of autocorrelation on the correlation analysis were also tested using effective number of degrees of freedom (N_{eff}) (at $p < 0.05$) (Bretherton et al., 1999). The results indicated negligible autocorrelation effects on the reported correlations (for the correlation coefficients in Tables 4 and 6), and thus the correlations can be considered statistically robust.

For the 1957–2013 CE period, the following climate indices were compared with the annual means of the GV7-C ice core records: station-based SAM index (Marshall G and National Center for Atmospheric Research Staff, 2018), the Southern Oscillation Index (SOI) (https://www.ncei.noaa.gov/access/monitoring/enso/soi), Niño3.4 index (https://psl.noaa.gov/gcoswgsp/Timeseries/Nino34), Indian Ocean Dipole (IOD) index representing the SST gradient between the western and southeastern equatorial IO (https://psl.noaa.gov/gcos_wgsp/Timeseries/DMI), SST anomaly in the southeastern IO (SST-SEIO) (https://psl.noaa.gov/gcos_wgsp/Timeseries/DMI), and reconstructed sea ice extent (SIE) over the Ross–Amundsen Sea sector (162°E–250°E) and the East Antarctic sector (71°E–162°E) (Fogt et al., 2023). Moreover, for the 1957–2013 CE period, spatial correlation analyses (at 95% confidence interval) were conducted between annual GV7-C records and gridded ERA5 reanalysis data (air temperature, SST, sea ice concentration [SIC], 10-m wind speed, zonal [u] and meridional [v] wind components, and total precipitable water) using Climate Reanalyzer developed by the University of Maine, USA (https://climatereanalyzer.org/). Since ice-core isotopic signals reflect a broad range of thermodynamic and dynamic influences, spatial correlation analyses were conducted for physically plausible scenarios to

help identify potential moisture supply regions over a longer time period (1957–2013 CE) than previous studies (Caiazzo et al., 2017; Khan, 2019). Spatially coherent and physically interpretable patterns are selectively presented and used as supportive evidence in the interpretation of climate-related signals from the GV7-C ice core. Principal component analysis (PCA), a linear dimensionality reduction technique, was employed to investigate potential similarities in variability between the annual means of the ice-core records and seasonal and annual means of climate datasets (IOD, SST-SEIO, SAM, SOI, Niño3.4, SIE) for 1957–2013 CE. The PCA results conducted on annual mean values were selected and presented in this study. For the 1872–2013 CE period, the GV7-C ice core data were compared with the IOD index, SST-SEIO, reconstructed SST anomaly over the Southern Hemisphere (https://www.ncei.noaa.gov/access/monitoring/climate-at-a-glance/global/time-series) (Huang et al., 2017), reconstructed SAM index (https://psl.noaa.gov/data/20thC_Rean/timeseries/monthly/SAM), and Niño3.4. SAM and ENSO are considered key modes potentially affecting Antarctic climate variability (Turner et al., 2009; Cohen et al., 2012; Pohl et al., 2021; Wille et al., 2021), and the SOI and Niño3.4 indices describe Pacific variability that can influence the climate of the Southern Ocean and Antarctica (Meyerson et al., 2002; Bertler et al., 2004). Moreover, the temperature anomalies (IOD index, SST-SEIO) over the Indian Ocean affects the air temperature (Zhang and Duan, 2023), sea ice extent (Kim et al., 2023; Zhang et al., 2024) and precipitation in Antarctica (Lee et al., 2024).

3 Results and discussion

3.1 Characterization of the GV7-C ice core record

The descriptive statistics for the annual mean $\delta^{18}O$, δD, *d*-excess, and SA in the GV7-C ice core are presented in Table 1. The results are also presented in five different time scales at around 50-year intervals (Table 1). Linear regression of $\delta^{18}O$ with δD and *d*-excess were reported for all data and the five different time scales, as well as for annually averaged values, annual maxima, and annual minima (Table 2). For the whole 1782–2013 CE period, the annual mean $\delta^{18}O$ in the GV7-C ice core (n = 233) fluctuated between –32.92‰ and –24.60‰, while δD ranged from –259.42‰ to –210.21‰. The annual variation in $\delta^{18}O$, *d*-excess, and SA is presented in Figure 2, revealing large interannual and decadal-scale variations. Sequential years (at least five) with smaller (or colder) than average $\delta^{18}O$ (–29.64‰) were observed for seven periods (1838–1842 CE, 1858–1862 CE, 1880–1885 CE, 1904–1908 CE, 1918–1922 CE, 1960–1965 CE, and 1995–2002 CE). Additionally, the years between 1977 CE and 1991 CE were lower than average, except for 1979 CE, 1982 CE, 1985 CE, and 1990 CE. In addition, sequential years (at least six) higher than the average were observed for 1787–1801 CE, 1807–1813 CE, 1937–1942 CE, and 1948–1958 CE (except 1953) (Fig. 2). The linear relationship between $\delta^{18}O$ and δD ($\delta D = 8.46 \times \delta^{18}O + 17.97$, $R^2 = 0.99$, n = 1880, $p < 0.001$) had a slope slightly larger than that for the precipitation isotopic composition both globally (8) (Craig, 1961) and on the Antarctic–wide scale (7.75) (Masson-Delmotte et al., 2008). The slopes derived for the different time scales ranged from 8.35 (for 1982–2013 CE) to 8.67 (for 1882–1931 CE) (Table 2).

The annual *d*-excess ranged between 1.70‰ and 7.61‰ (n = 233) (Table 1). Periods with values larger than the mean for at least five sequential years were observed for 1786–1790 CE, 1855–1861 CE, 1884–1888 CE, 1903–1911 CE, 1932–1940 CE, 1951–1956 CE, 1962–1966 CE, and 1974–1978 CE, while years with lower values than the mean for at least five sequential years occurred in 1798–1802 CE, 1840–1848 CE, 1922–1926 CE, 1985–1990 CE, and 2006–2011 CE (Fig. 2). A positive correlation was observed between $\delta^{18}O$ and *d*-excess (r = 0.45, $p < 0.001$, n = 1880) (Table 2), indicating their relevance to the climatic conditions in the moisture source region. The slopes for the relationship between *d*-excess and $\delta^{18}O$ varied slightly between different time periods, though positive correlations were consistently maintained over these periods (Table 2). This suggests a relatively consistent supply of the air mass source (i.e., oceanic) to the GV7-C site. It can be assumed that the variation in $\delta^{18}O$ and *d*-excess in the GV7-C ice core is indicative of the oceanic surface conditions (e.g., humidity, SST, and wind speed) (Uemura et al., 2008).

The annual mean SA ranged from 79 to 460 mm w.e. yr^{-1} in the GV7-C ice core, with a long-term mean of 223 ± 59 mm w.e. yr^{-1} (Table 1). Strong interannual variation was observed, with no long-term trend over the 1782–2013 CE period. Consecutive years (at least four) with a SA larger than the mean (223 mm w.e. yr^{-1}) were observed in 1784–1787 CE, 1896–1899 CE, and 1999–2002 CE, while the 1878–1883 CE and 1945–1952 CE periods exhibited a lower SA rate than the mean (Fig. 2). The mean SA in the GV7-C ice core was comparable to previously reported records nearby and in other coastal regions across East Antarctica (Table 3).

Table 1. Descriptive statistics for the annual means of the GV7-C ice core data.

Years (CE)	Long-term (1782–2013)	1782–1831	1832–1881	1882–1931	1932–1981	1982–2013
			$\delta^{18}O$ (‰)			
Mean	–29.64	–29.24	–29.78	–29.88	–29.49	–29.90
Standard Deviation	1.26	1.02	1.41	1.09	1.28	1.45
Minimum	–32.92	–32.72	–32.92	–32.34	–32.74	–31.96
Maximum	–24.60	–26.86	–24.60	–27.39	–27.14	–24.84
			δD (‰)			
Mean	–232.69	–229.59	–233.76	–234.69	–231.76	–234.17
Standard Deviation	10.37	8.42	11.50	9.31	10.50	11.91
Minimum	–259.42	–259.42	–258.36	–255.61	–258.98	–250.66
Maximum	–191.43	–210.21	–191.43	–213.50	–212.01	–192.08
			d-excess (‰)			
Mean	4.43	4.33	4.44	4.36	4.20	5.02
Standard Deviation	1.07	0.88	1.08	1.25	1.03	0.97
Minimum	1.70	2.25	2.21	1.70	2.42	2.98
Maximum	7.61	6.34	6.99	7.61	7.07	6.64
			Snow accumulation (mm w.e. yr^{-1})			
Mean	223.01	225.06	217.80	227.03	219.76	226.70
Standard Deviation	58.77	68.97	48.93	54.91	59.15	63.50
Minimum	79.02	101.79	143.06	81.37	107.58	79.02
Maximum	459.88	459.88	307.94	319.04	340.61	343.92

Table 2. Linear regression analysis for $\delta^{18}O$ with δD and *d*-excess from the GV7-C ice core.

	Slope	Intercept	R^2	*p*-value	n
		$\delta^{18}O$ vs δD			
1782–2013 CE (all data)	8.46	17.97	0.99	<0.0001	1880
1782–1831 CE	8.54	20.12	0.99	<0.0001	344
1832–1881 CE	8.44	17.60	0.99	<0.0001	355
1882–1931 CE	8.67	24.36	0.99	<0.0001	399
1932–1981 CE	8.51	19.41	0.99	<0.0001	429
1982–2013 CE	8.35	15.51	0.99	<0.0001	353
Annual mean	8.17	9.64	0.99	<0.0001	233
Annual maximum	8.27	13.57	0.98	<0.0001	233
Annual minimum	8.19	9.07	0.99	<0.0001	233
		$\delta^{18}O$ vs *d*-excess			
1782–2013 CE (all data)	0.46	18.07	0.21	<0.0001	1880
1782–1831 CE	0.54	20.04	0.24	<0.0001	344
1832–1881 CE	0.45	17.83	0.18	<0.0001	355
1882–1931 CE	0.67	24.33	0.34	<0.0001	399
1932–1981 CE	0.52	19.45	0.24	<0.0001	429
1982–2013 CE	0.36	15.62	0.18	<0.0001	353
Annual mean	0.18	9.68	0.04	<0.0001	233
Annual maximum	0.28	14.45	0.10	<0.0001	233
Annual minimum	0.26	10.68	0.09	<0.0001	233

185

Table 3. Comparison of the mean snow accumulation rate from the GV7-C ice core with previous ice core records in this location and other East Antarctic ice cores.

Location	Approximate distance to GV7-C, km	Snow accumulation, mm w.e yr^{-1}	Period (CE)	Reference
GV7-C	–	223 ± 59	1782–2013	This study
GV7 site	–	252 ± 104	2001–2004	Frezzotti et al., 2007
GV7 site	–	242 ± 71	2007–2013	Caiazzo et al., 2017
GV7 site	–	250 ± 85	2008–2013	Caiazzo et al., 2017
GV7 site	–	238.7 ± 13	1979–2012	Khan, 2019
GV7 site	–	241 ± 13	1965–2001	Magand et al., 2004
GV7 site	–	242 ± 57	1965–2000	Nardin et al., 2021
GV7 site	–	233 ± 64	1854–2004	Nardin et al., 2021
GV7 site	–	205 ± 63	1179–2009	Nardin et al., 2021
RICE	972	210	1965–2017	Winstrup et al., 2017
Mt. Erebus Saddle	811	230	1950–2006	Rhodes et al., 2012
Styx-B	394	146 ± 60	1990–2014	Nyamgerel et al., 2020
Hercules Névé	348	119	1770–1992	Stenni et al., 1999
VLG (Victoria Lower Glacier)	155	30	1808–2000	Bertler et al., 2011
Talos Dome	239	80	1232–1995	Stenni et al., 2002
Adelie Land	884	218 ± 69	1946–2006	Goursaud et al., 2017
Law Dome	1855	688	22 BCE to 2012	Roberts et al., 2015
Aurora Basin North	1713	119	1979–2013	Servettaz et al., 2020
Mount Brown South	2648	263 ± 46	1979–2016	Jackson et al., 2023

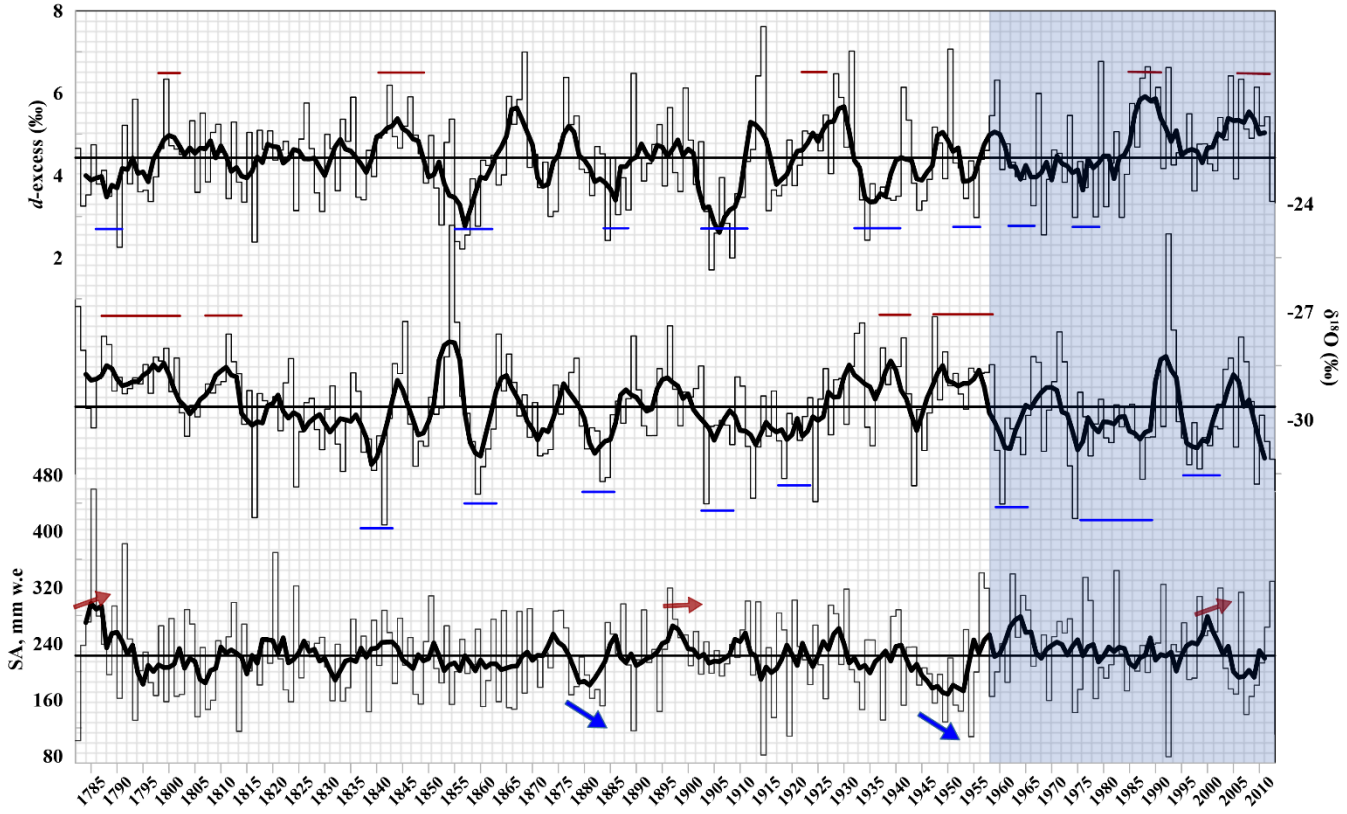


Figure 2. Temporal variation in the SA (bottom panel), $\delta^{18}O$ (middle panel), and *d*-excess (top panel), with the horizontal black line indicating the overall mean. The thick black lines represent the 5-year running average. The blue and red lines (arrows) indicate the periods that are lower or higher than average for at least four continuous years. Blue shadow represents the 1957–2013 CE period that discussed in section 3.2.

3.2 Spatial correlation analysis with ERA5 reanalysis

Spatial correlation analyses (95% confidence interval) were conducted between annual GV7-C records ($\delta^{18}O$, *d*-excess, and SA) and annual/seasonal ERA5 reanalysis fields for 1957–2013 CE to explore potential spatial patterns consistent with moisture supply and transport pathways. Significant and physically interpretable patterns are selectively presented in the Supplement (Figs. S1–S3) and are used as supporting evidence in the discussion of likely source regions. For interpretation, the Pacific Ocean (PO) sector is defined here as the western Pacific (90–160°E), Ross Sea (160°E–130°W), and Amundsen–Bellingshausen Seas (130–60°W), while the Indian Ocean (IO) sector is defined as 20–90°E.

Annual mean $\delta^{18}O$ shows positive correlations with 2 m air temperature and SST primarily over the PO sector (Fig. S1a, b). Positive relationships with air temperature (2 m and 850 hPa) and total column precipitable water are most evident during DJF over parts of the PO and IO sectors (Fig. S1d–f). Negative correlations are observed with sea ice concentration (SIC) over the Ross Sea region (Fig. S1c). Wind-speed correlations (10 m; annual and MAM) are generally negative (Fig. S1g, j), and zonal wind (u-wind) correlations highlight the belt of strong westerlies (Fig. S1h, k). The meridional wind (v-wind) correlations suggest a northward flow signature from the western PO sector and a southward flow signature from the IO sector during DJF (Fig. S1i), whereas these patterns weaken in MAM (Fig. S1l). Overall, $\delta^{18}O$ exhibits its clearest spatial coherence during DJF and MAM, consistent with the seasonality of transport and snowfall in this coastal sector (Delmotte et al., 2000; Caiazzo et al., 2017). These patterns provide qualitative support for a relatively stronger PO-sector influence on $\delta^{18}O$ at GV7-C during DJF–MAM, although the overall relationships remain modest.

Annual mean *d*-excess exhibits positive correlations with air temperature (2 m and 850 hPa) over both the western PO and IO sectors (Fig. S2a–c). Temperature correlations in the IO sector are particularly evident in SON (Fig. S2c), whereas the *d*-excess response to temperature appears weaker in DJF (not shown). Correlations with SST (SON), SIC (JJA), and total column precipitable water (annual) further support a contribution of air masses from the IO sector and western PO to the GV7 region (Fig. S2d–f). In contrast to $\delta^{18}O$, correlations with wind speed and wind direction are relatively weak, except for a positive correlation with 10 m wind speed in some regions (Fig. S2g). The v-wind pattern indicates a southward flow signature from the IO sector and a northward flow signature in the western PO sector (Fig. S2i). Taken together, these spatial patterns suggest that thermodynamic source-region variability (e.g., SST/air-temperature conditions) may play a comparatively larger role for *d*-excess at GV7-C than do purely dynamical indicators, and they are consistent with a potentially important contribution from the IO sector, particularly during SON.

No clear and temporally consistent relationships are observed between SA and the investigated climate variables; only weak and spatially limited patterns are identified (Fig. S3). For example, SA shows weak negative correlations with 2 m temperature over parts of the Amundsen Sea coast and weak positive correlations with total column precipitable water offshore of the Ross Sea coast (Fig. S3a, b). SA also shows weak negative correlations with SIC over the Ross Sea region (Fig. S3c). Wind-speed correlations (10 m and 850 hPa) are weakly positive over parts of the PO sector (Fig. S3d, g), and the associated

u- and v-wind patterns suggest modest transport signals (Fig. S3e, f, h, i). Overall, these results indicate that SA at GV7-C is likely influenced by multiple factors, including synoptic variability and transport efficiency, which may mask simple relationships with large-scale indices at annual resolution.

In sumumary, the results from the spatial correlation analysis suggest that the GV7-C ice core can be used to represent the regional climate conditions over the PO and IO sector. The correlations observed with $\delta^{18}O$ during the DJF and MAM seasons led us to consider the potential influence of the SAM. It is conceivable that a positive phase of SAM during the DJF and MAM seasons could strengthen the climate signals, allowing SAM-related signals to be detectable in $\delta^{18}O$ and SA during the 1957–2013 CE period. The dynamic influence of SAM can thus be important for $\delta^{18}O$ and SA, while *d*-excess is likely to represent thermodynamic changes over the IO and western PO sectors, particularly during the SON season. These correlations for *d*-excess can be remotely connected to the temperature variability over the tropical IO and PO (Masson-Delmotte et al., 2003).

3.3 Correlation analysis for 1957–2013 CE and 1872–2013 CE periods

3.3.1 Climate signals for the 1957–2013 CE period

The SAM, Niño3.4, SOI, IOD, SST-SEIO, and SIE data were compared with the $\delta^{18}O$, *d*-excess, SA of the GV7-C ice core. The standardized values of the variables for 1957–2013 CE are presented in Figure 3. The $\delta^{18}O$ exhibited three periods of higher values (1964–1971 CE, 1989–1993 CE, and 2001–2007 CE) (Fig. 3), while the *d*-excess remained generally flat before 1983 and showed two periods of higher values (1985–1992, 2002–2011). The SA values showed significant interannual variations. Pearson's correlation coefficients (r) between the GV7-C ice core records and the climate variables are shown in Table 4. Correlations are calculated for annual and three-year running averages in detrended time series. Correlations on original time series were also shown as comparison to the detrended results, and the results were comparable (Table 4). For the annual mean time series, no significant correlations were found, except that SA show a weak correlation to IOD ($r = 0.37$, $p < 0.05$, $n = 57$). Furthermore, SA kept weak positive correlations with IOD ($r = 0.39$, $p < 0.01$ $n = 55$) and SST-SEIO ($r = –0.30$, $p < 0.05$ $n = 55$) in the three-year running averaged time series. While the $\delta^{18}O$ exhibited correlations with SAM ($r = –0.41$, $p < 0.005$, $n = 55$), SOI ($r = –0.49$, $p < 0.001$, $n = 55$), Niño3.4 ($r = 0.46$, $p < 0.001$, $n = 55$), and SIE over the Ross-Amundsen Sea ($r = –0.47$, $p < 0.001$, $n = 55$) in the three-year running-averaged time series. For *d*-excess, there was a moderate correlation with SST-SEIO ($r = 0.64$, $p < 0.001$ $n = 55$), and weak correlations with the IOD ($r = –0.45$, $p < 0.001$, $n = 55$), and SIE over the East Antarctic sector ($r = –0.35$, $p < 0.001$, $n = 55$). Overall, the correlation analysis likely to suggest the variations in the $\delta^{18}O$ (for the 1957–2013 CE) capture the climatic signals over the tropical PO as well as the southern sector of the PO, indicating the contribution of air mass originating from this region. While the *d*-excess likely to indicates the climatic signals (sea surface temperature) over the southeastern IO, and this relevance indicate the air mass intrusion from this region. Moreover, the climatic conditions over the Indian Ocean sector appear to have reflected in the SA of the ice core.

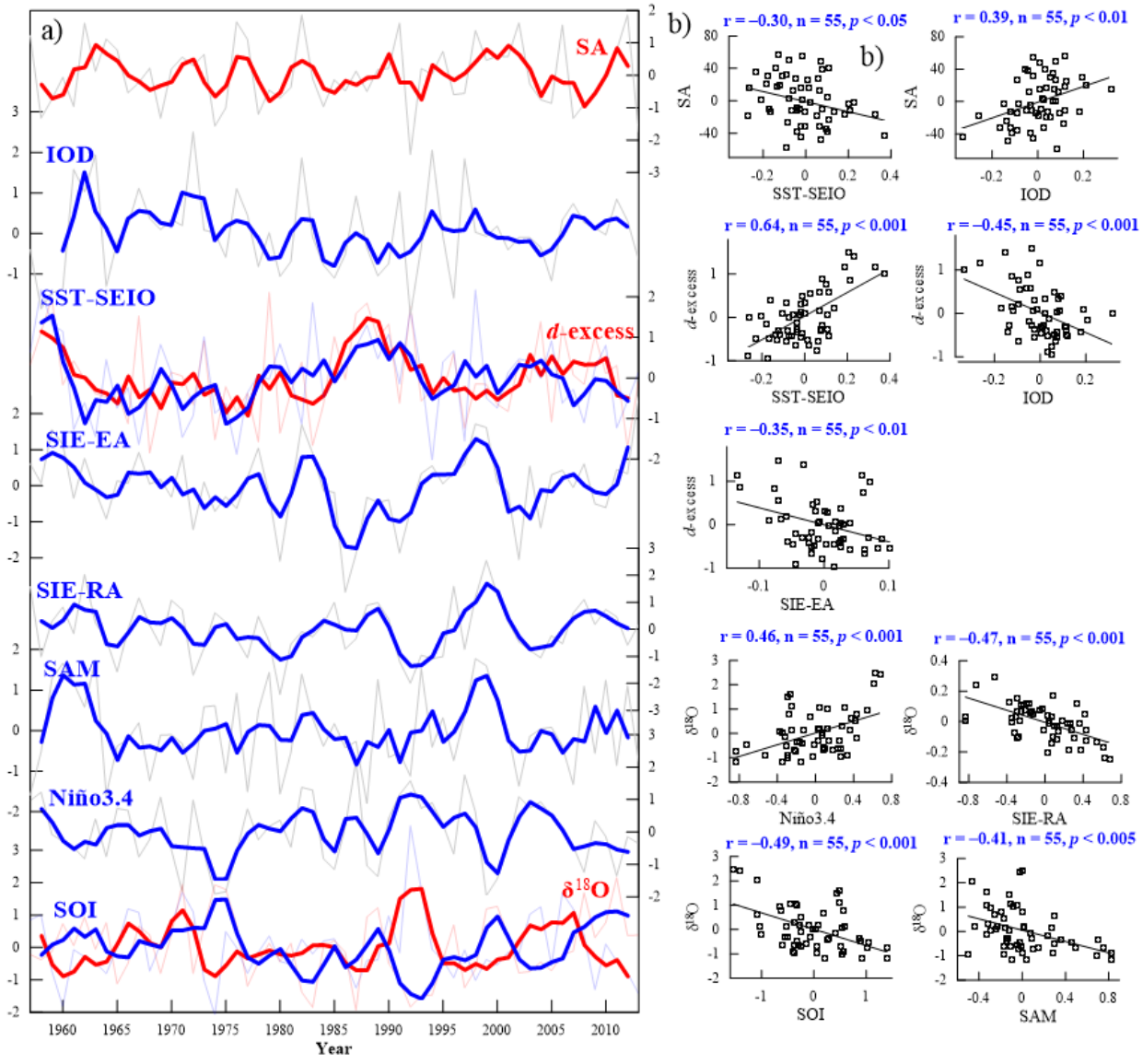
PCA analysis conducted for 1957–2013 CE, with the loading matrix (correlation coefficients at $p < 0.05$) presented in Table 5. Principal component (PC) 1 clustered $\delta^{18}O$, the SAM, SOI, Niño3.4, and SIE over the East Antarctica and Ross-Amundsen Sea region. This reflected the importance of both thermodynamic and dynamic effects on the decrease (increase) in $\delta^{18}O$ with an increase (decrease) in the SIE, stronger (weaker) westerly winds (i.e., the SAM and SOI), and lower (higher) SSTs in the Niño3.4 region. In PC 2, *d*-excess and SA were clustered with IOD, SAM, SIE, and particularly strong signal of SST-SEIO. This can represent the increasing (decreasing) *d*-excess with increased (decreased) evaporation with warm (cold) SSTs particularly over the southeastern IO. Moreover, there could be a weak relevance with enhanced (weakened) air mass transport with strong westerlies (i.e., the SAM), consequent wind-induced increase (decrease) in SIE over East Antarctica and relatively cooler temperature over the eastern IO (decreasing IOD). It is ambiguous to explain the negative correlation between the SA and SST-SEIO in PC 2. However, PC 3 included SA only, with more stronger signals of IOD, SAM, SOI, Niño3.4 and SIE over the East Antarctica. This can represent the thermodynamic effects on SA with increased (decreased) evaporation with warm SSTs over western equatorial IO and central tropical PO (i.e., the SOI and Niño3.4), enhanced moisture transport with strong westerlies (i.e., the SAM), and the wind-induced SIE over East Antarctica. PC 4 was characterized by an increasing (decreasing) $\delta^{18}O$, *d*-excess with decreasing (increasing) SST-SEIO which can be explained by the intrusion of different air masses with evident *d*-excess signals together with $\delta^{18}O$. Overall, PCA classified the variables into species representing the climatic signals corresponding to the PO (PC 1) and southeastern IO sector of the Southern Ocean (PC 2). Interestingly, the relatively strong detectability of the thermodynamic effect on *d*-excess, which is induced by the IO sector, likely to indicate the significant (detectable) temperature signals in this region.

Table 4. Pearson's correlation coefficients (r) between the GV7-C ice core records and the climate variables for the period 1957–2013 CE. Correlations are calculated for annual data and three-year running averages in the detrended and original time series (shown in parentheses). Larger values (r > 0.3 at $p < 0.05$) are marked in bold. SIE (EA) and SIE (RA) denotes sea ice extent over East Antarctica and the Ross-Amundsen Sea sector.

	IOD	SST (SEIO)	SAM	SOI	Niño3.4	SIE (EA)	SIE (RA)
				Annual average			
SA	**0.37** (0.28)	–0.22 (–0.26)	0.12 (0.04)	–0.00 (–0.01)	0.04 (0.04)	0.01 (–0.02)	0.09 (0.00)
$\delta^{18}O$	–0.01 (–0.03)	–0.06 (–0.07)	–0.18 (–0.18)	–0.26 (-0.26)	0.22 (0.22)	–0.06 (–0.07)	–0.23 (–0.22)
d-excess	–0.19 (–0.07)	0.25 **(0.33)**	–0.03 (0.09)	0.02 (0.03)	0.04 (0.05)	–0.05 (0.02)	0.11 (0.22)
				Three-year running average			
SA	**0.39** (0.18)	**–0.30 (–0.36)**	0.11 (–0.06)	0.09 (0.09)	–0.11 (–0.14)	0.11 (0.04)	–0.18 (–0.02)
$\delta^{18}O$	–0.06 (–0.02)	0.02 (0.04)	**–0.41** (–0.27)	**–0.49 (–0.49)**	**0.46 (0.46)**	–0.14 (–0.11)	**–0.47 (–0.32)**
d-excess	**–0.45** (–0.06)	**0.64 (0.72)**	–0.15 (–0.21)	–0.11 (–0.09)	0.24 (0.27)	**–0.35** (–0.16)	0.01 (0.31)

Table 5. Loadings of the variables for the first four principal components (PCs) of the PCA analysis conducted with the data for 1957–2013 CE. Larger values of correlation coefficients (r > 0.3, at $p < 0.05$) are marked in underlined bold.

Variables	PC1	PC2	PC3	PC4
SA	0.04	**–0.48**	**0.43**	–0.04
$\delta^{18}O$	**–0.39**	0.20	–0.04	**0.77**
d-excess	0.05	**0.63**	–0.07	**0.49**
IOD	0.12	**–0.30**	**0.77**	0.27
SST-SEIO	–0.07	**0.82**	–0.08	**–0.40**
SAM	**0.52**	**0.30**	**0.56**	–0.08
SOI	**0.82**	–0.23	**–0.43**	0.13
Niño3.4	**–0.80**	0.27	**0.47**	–0.13
SIE (EA)	**0.52**	**0.31**	**0.38**	0.00
SIE (RA)	**0.84**	0.29	0.13	0.05
Variance explained (%)	*27*	*18*	*17*	*11*
Cumulative percent (%)	*27*	*45*	*62*	*73*



290

Figure 3. Comparison of the standardized profiles (grey lines) for detrended time series of SA, $\delta^{18}O$, and *d*-excess with the climate variables for 1957–2013 CE (a). The thick lines (blue and red) indicate the 3-year running average. Linear regression profiles for the 3-year running averaged time series are also shown with significant correlation coefficients (at $p < 0.05$) (b).

3.3.2 Climate signals for the long-term records (1872–2013 CE)

The GV7-C ice core data were also compared with long-term records (1872–2013 CE) for the SAM, Niño3.4, IOD, SST-SEIO, and SST anomaly over the Southern Hemisphere (Fig. 4 and Table 6). Pearson's correlation coefficients (r) between the GV7-C ice core records and the climate variables are shown in Table 4. Correlations are calculated for annual and three-year running averages in detrended time series. Correlations on original time series were also shown as comparison to the detrended results, and the results were comparable (Table 6). For the $\delta^{18}O$ and SA, no significant correlations were found with the climate variables in this period. This disappearance suggesting the smoothing of signal intensity due to various influencing factors. Considering the correlation of $\delta^{18}O$ with Niño3.4 ($r = 0.46$) and SOI ($r = -0.49$) for 1957–2013 CE (Table 4), this suggests the influence of SST changes in the PO sector. However, this correlation weakened over a longer period (1872–2013). However, some evident relevance can still be observed in the short-term period for $\delta^{18}O$ and SA. The decrease in SA during the 1876–1885 CE and 1940–1955 CE periods was consistent with the increasing trend in the SAM. The recent trend (1985–2013) for $\delta^{18}O$ was also found to be in line with Niño3.4 and the SAM index (Fig. 4). While the *d*-excess was correlated with SST-SEIO ($r = 0.32$, $n = 140$, $p < 0.001$) in the three-year averaged time series. (Table 6 and Fig. 4). The spatial correlation of *d*-excess with the reconstructed SST dataset was also tested for two periods: 1957–2013 CE, and 1854–2013 CE (Fig. 5). Weak positive correlations were observed over the remote IO sector during the 1957–2013 CE period (Fig. 5a) while in the period from 1854 to 2013 CE, the correlation was observed over a larger area in the southern sector of the IO (Fig. 5b). Therefore, the *d*-excess signal from the GV7-C ice core can be roughly suggested to representing thermodynamic changes (i.e., SST changes) over the IO sector of the Southern Ocean, at least over the 1872–2013 CE period.

315

Table 6. Pearson's correlation coefficients (r) between the GV7-C ice core records and the climate variables for the period 1872–2013 CE. Correlations are calculated for annual data and three-year running averages in the detrended and original time series (shown in parentheses). Larger values ($r > 0.3$ at $p < 0.05$) are marked in underlined bold.

	IOD	SST (SEIO)	SST anomaly	SAM	Niño3.4
			Annual average		
SA	0.10 (0.10)	–0.15 (–0.11)	–0.03 (–0.01)	0.03 (0.03)	0.02 (0.02)
$\delta^{18}O$	–0.04 (–0.04)	–0.01 (–0.02)	–0.10 (–0.08)	–0.16 (–0.14)	0.14 (0.13)
d-excess	–0.02 (0.08)	0.02 (0.28)	–0.20 (0.28)	0.06 (0.18)	0.12 (0.13)
			Three-year running average		
SA	–0.04 (0.01)	–0.02 (0.02)	–0.04 (0.02)	0.00 (0.04)	0.02 (0.03)
$\delta^{18}O$	–0.12 (–0.11)	0.00 (–0.02)	–0.13 (–0.11)	–0.23 (–0.16)	0.19 (0.18)
d-excess	0.03 (0.23)	**0.32 (0.43)**	0.26 **(0.39)**	–0.02 (0.24)	0.24 (0.26)

320

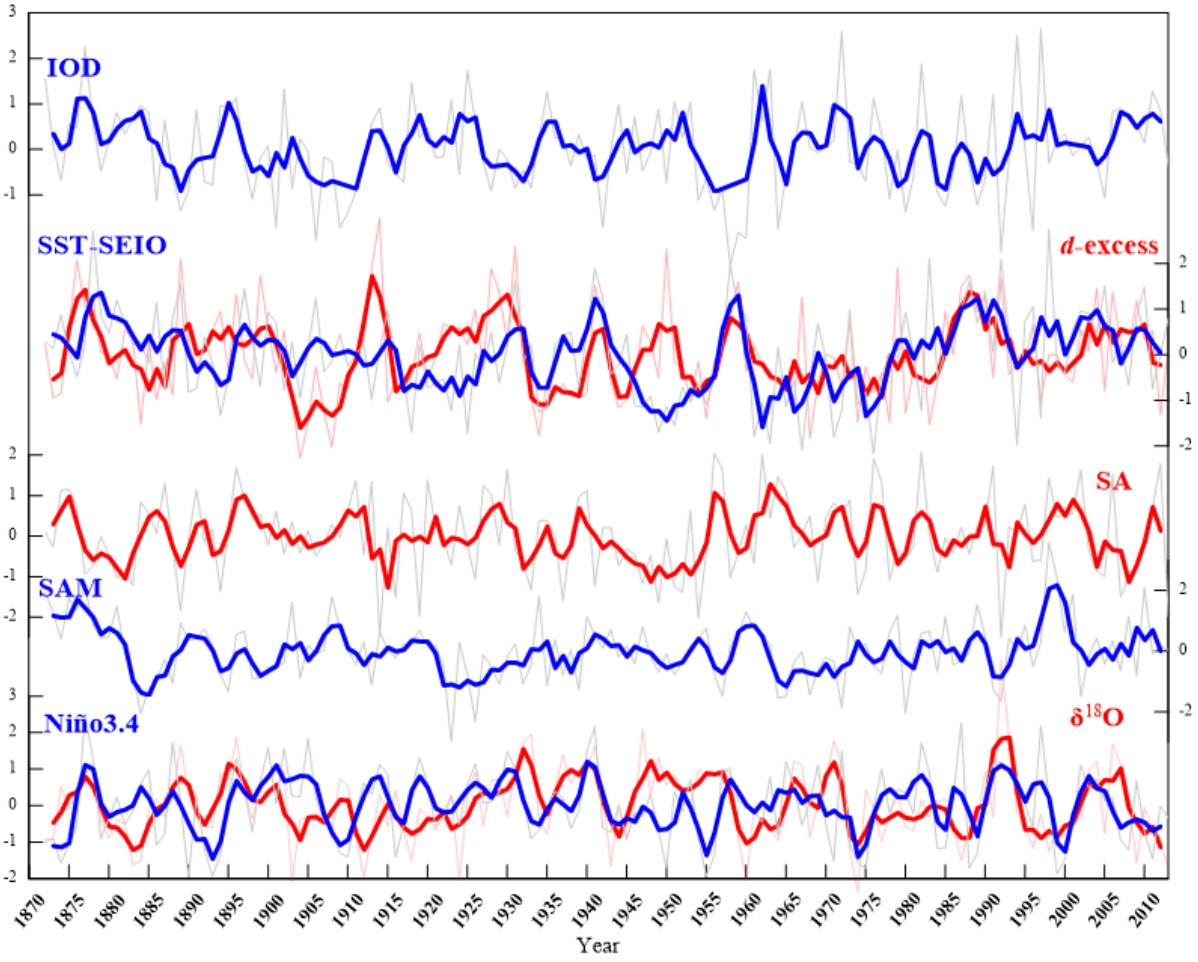


Figure 4. Comparison of the standardized profiles (thin lines) for detrended time series of SA, $\delta^{18}O$, and *d*-excess with the IOD, SST anomaly of the southeastern Indian Ocean (SST-SEIO), SST anomalies over the Southern Hemisphere, the SAM, and Nino3.4 for 1872–2013 CE. The thick lines (blue and red) indicate the 3-year running average

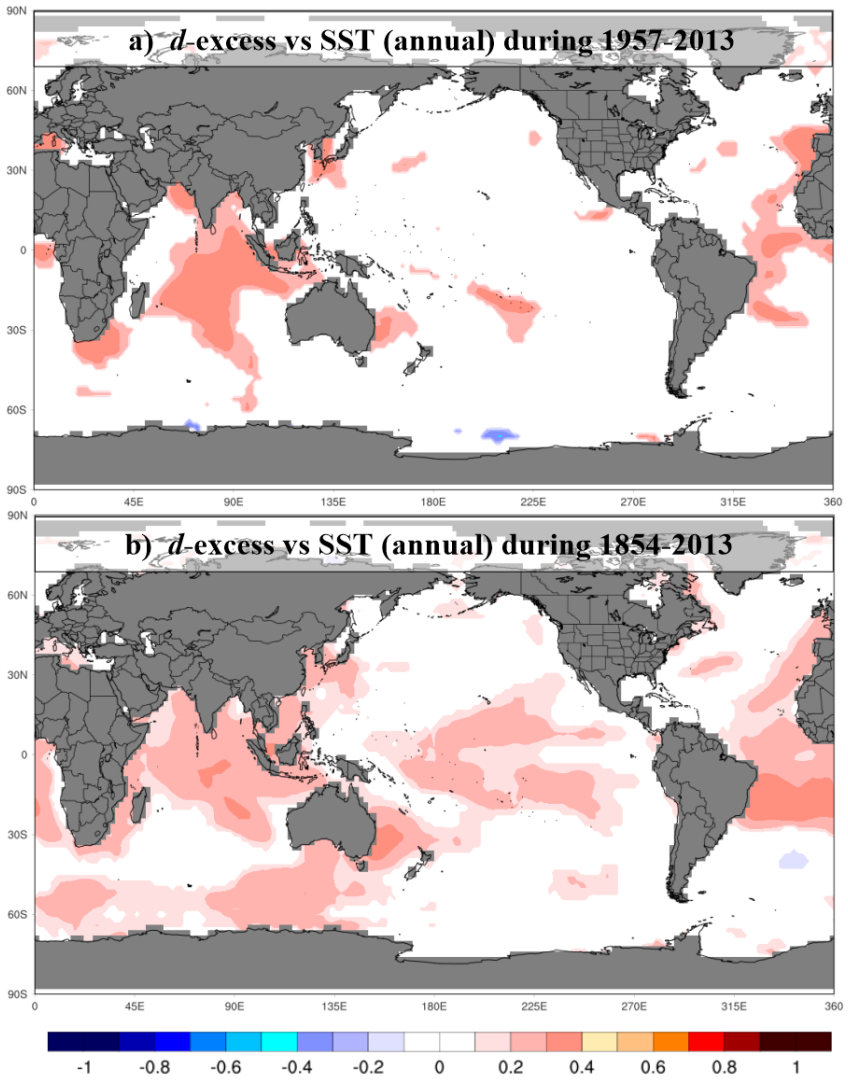


Figure 5. Spatial correlation of *d*-excess with annual SST variability for (a) 1957–2013 CE and (b) 1854–2013 CE. The scale bars indicate Pearson's correlation coefficient (r) at $p < 0.05$. This figure was generated using Climate Reanalyzer (https://climatereanalyzer.org/) from the Climate Change Institute, University of Maine, USA.

330

3.4 Discussion and implications

The variations in SA data from the GV7-C ice core showed significant interannual variations, and show only a weak correlation with IOD and SST-SEIO. The SA of the GV7-C ice core is assumed to be affected by the coupled influence of dynamic processes (i.e., the transport pathways and transport efficiency of moist air) or abrupt synoptic events (e.g., intense transport by atmospheric river events) (Turner et al., 2019; Wille et al., 2021). The variability in SA is affected by moisture transport via large-scale atmospheric circulation (Thomas et al., 2008; Udy et al., 2021; Cohen et al., 2012) and synoptic-scale short-lived events (e.g., atmospheric river events, atmospheric rivers) (Turner et al., 2019; Wille et al., 2021) and evident in the ice core records from coastal regions (Servettaz et al., 2020; Jackson et al., 2023). Moreover, the intensity and frequency of cyclone events also affect snowfall in Antarctic coastal areas (Dalaiden et al., 2020a). Particularly, in the Ross Sea region, the cyclonically driven SA is dominant and the region is sensitive to tropical and local climate drivers (Bertler et al., 2018). The contribution of synoptic-scale transport has been reported to be large for Victoria Land based on simulations over the 1985–2014 period (Dalaiden et al., 2020a). The influence of the ENSO on SA was evident at the Law Dome site (Roberts et al., 2015).

Based on the correlation of $\delta^{18}O$ in the GV7-C ice core with Nino 3.4, SOI, SAM, and SIE over the Ross-Amundsen Sea sector for 1957–2013 CE, the increasing (decreasing) $\delta^{18}O$ can be partly explained by the intrusion of relatively warm (colder) and moist (dry) air mass mainly through the PO sector of the Southern Ocean. This finding is comparable to other ice cores from the coastal Antarctica. In the Mount Brown South ice core in East Antarctica, evidence for moisture transport from the southern IO has been detectable from $\delta^{18}O$ signal, and the extreme precipitation events are linked with high-pressure systems in the mid-latitudes which increase the transport of warm and moist air mass from the southern IO (Jackson et al., 2023). In another ice core from Adélie Land covering the 1946–2006 CE period, decadal variations in $\delta^{18}O$ and regional temperature were correlated (Goursaud et al., 2017). Moreover, $\delta^{18}O$ shows a tendency to decrease with increasing wind speed. However, the $\delta^{18}O$ on an annual scale could not be explained by changes in the SIE and temperature, indicating the importance of site-dependent climate signals in coastal ice cores (Goursaud et al., 2017). In another study, isotope-based results indicated colder SSTs, a higher SIE, stronger katabatic winds, and decreasing SA in the Victoria Low Glacier ice core during the 1288–1807 period (the Little Ice Age period) (Bertler et al., 2011). Little Ice Age-related cooling is also evident in the $\delta^{18}O$ signal from the Hercules Neve ice core for the 1770–1890 period (Stenni et al., 1999) and frequent cold intervals in the Talos Dome ice core (Stenni et al., 2002). In line with these observations, a slight decreasing trend was observed in the $\delta^{18}O$ signal from the GV7-C ice core during the 1782–1845 CE period (Fig. 4), which may be part of Little Ice Age cooling. After 1845, there was no long-term trend in $\delta^{18}O$ from the GV7-C ice core; rather, values lower than the long-term mean were frequently observed (the blue lines in Fig. 4). This depletion of $\delta^{18}O$ observed from the GV7-C ice core may be possibly linked with changes in atmospheric circulation (e.g., SAM-related cooling) (Thompson and Solomon, 2002). Moreover, in terms of temperature reconstruction, $\delta^{18}O$ signal in the GV7-C ice core contrasts to anthropogenic global warming, suggesting more local/regional variations or various climatic factors.

Based on the correlation of *d*-excess with SST-SEIO and SST anomaly (Tables 4 and 6), the *d*-excess signal from the GV7-C ice core likely to preserve the thermodynamic changes (i.e., SST changes) particularly over the IO sector of the Southern Ocean. Notably, the southern Indian Ocean exhibits the most intense cyclonic activity in the Southern Ocean, which may enhance the detectability of this signal in the *d*-excess record (Simmonds et al., 2003). *D*-excess as an indicator of climate conditions in the source region (Jouzel et al., 1982; Sodemann and Stohl, 2009; Lewis et al., 2013), warming over the Southern Ocean, was found to co-vary with higher *d*-excess in the Victoria Lower Glacier ice core (Bertler et al., 2011). At the Law Dome ice core site, *d*-excess also reflects SST changes over the southern IO sector (Masson-Delmotte et al., 2003). Particularly the abrupt increase in the *d*-excess in the 1970s was consistent with the *d*-excess of the GV7-C ice core. This relevance was explained by the abrupt changes in meridional atmospheric circulation, which led to the intrusion of warm subtropical moisture sources to the Antarctic coast during the 1970s (Masson-Delmotte et al., 2003). Consistently large peaks in the five-year running averaged time series for *d*-excess (both high and low values) were more frequent after 1845 (Fig. 2). Furthermore, it can be reported that the increasing phases in the global average temperature during the 1910–1945 CE period and since 1976 (IPCC, 2001) are evident in the increasing trend for *d*-excess (Fig. 2). Changes in the SAM have also been linked to tropical SST changes and other tropical variabilities (Clem and Fogt, 2013; Ding et al., 2012). The climate signals in some coastal sites, including RICE, Mt. Erebus Saddle, and Styx Glacier, have been thought to be primarily indicative of local and regional conditions in the Ross Sea region (Rhodes et al., 2012, Nyamgerel et al., 2020, 2024). Similarly, the influence IOD on the eastern East Antarctic precipitation was more dominant than the SAM-induced changes for the 1979–2014 (Lee and Jin, 2024). The IOD-related variation in the precipitation is explained by waves originating from the Indian Ocean that propagate southeastward, and inducing a low-pressure anomaly near eastern east Antarctica, consequently reducing precipitation. Thus, in the GV7-C ice core site, variabilities linked to remote teleconnections with SST over the IO sector of the Southern Ocean were assumed to be associated with *d*-excess.

Based on various correlation analysis with the climate variables used in this study, the following interpretations are summarized. During the period 1957–2013 CE, the correlation patterns based on SA, δ18O, and d-excess support that snow precipitating at the GV7-C site mainly originates from the Southern Ocean possibly via western PO and southeastern Indian Ocean. For the longer time scale (1872–2013), the correlation patterns based on d-excess for SST indicates more detectability of air mass intrusion from the Indian Ocean sector of the Southern Ocean. This suggests a warmer (colder) ocean surface condition would be preserved in higher (lower) δ18O (recent period) and d-excess values (recent and longer period) in the GV7-C ice core, reflecting changes in moisture source conditions and evaporation processes prior to condensation. In particular, the enhanced sensitivity of d-excess to SST over longer timescales highlights its utility in tracing shifts in moisture source regions and atmospheric transport pathways. Together, these results indicate that $\delta^{18}O$ and d-excess provide complementary constraints on both thermal conditions and moisture source dynamics recorded in the GV7-C ice core.

Lastly, it is notable that the importance of the GV7-C ice core records in climate studies. The historical temperature variability over the tropical ocean is important for global warming scenarios (IPCC, 2019). The projections show oceanic and atmospheric warming (Timmermann and Hellmer, 2013), and heat transported by the Southern Ocean further induces the melting of Antarctic ice shelves (Rignot et al., 2019). Particularly, the IO is experiencing the strongest and most robust warming (Du and Xie, 2008; Beal et al., 2019), largely driven by anthropogenic forcing (Dong et al., 2014), and it is projected to warm non-uniformly (Sharma et al., 2023). The IO and the PO temperature anomaly affects the surface air temperature of Antarctica (Zhang and Duan, 2023). Moreover, warm SSTs in the western tropical IO excite a poleward-moving Rossby wave, inducing the changes in sea ice extent (Zhang et al., 2024). The coastal and inland Antarctic regions emerge an anomalous retreat of sea ice extent and warming due to the short-term significant intrusion of warm and moist air masses associated with strong negative phase of SAM (Ionita et al., 2018). The SAM variation in the recent period is unprecedented in the last millennia (Fogt and Marshall, 2020) and the increasing influence of the SAM-ENSO coupling has been reported since the 1940s (in coastal Dronning Maud Land) (Ejaz et al., 2022). Thus, understanding the response of the Antarctic climate to ocean variability of the IO sector would be important.

4 Conclusions

The $\delta^{18}O$, *d*-excess, and SA records from the GV7-C ice core in East Antarctica (1782–2013 CE) were analyzed to investigate potential links with large-scale climate variability. Snow accumulation shows significant interannual variability, likely reflecting the combined influence of transport pathways, synoptic events, and local processes, and is only weakly correlated with SST variability over the IO for 1957–2013 CE. In contrast, $\delta^{18}O$ and *d*-excess exhibit relatively detectable relationships with climate indices for 1957–2013 CE, including Niño3.4, SOI, SAM, IOD, SST-SEIO, and reconstructed sea ice extent over the Ross–Amundsen Sea sector and East Antarctic sector. Notably, *d*-excess shows a persistent relationship with SST-SEIO. Over the longer period (1872–2013 CE), $\delta^{18}O$ relationships generally weaken, suggesting time-varying controls, whereas *d*-excess retains correlations with SST-SEIO. Correlation patterns and spatial analyses suggest that moisture reaching GV7-C primarily originates from the Southern Ocean, with contributions from the western Pacific and southeastern Indian Ocean sectors during 1957–2013 CE, while IO-sector influence is more evident over longer timescales. Overall, the GV7-C record provides evidence for potential teleconnections between low-latitude ocean variability and coastal East Antarctic climate.

Code and data availability. Data reported in this study have been deposited at the Korea Polar Data Center (KPDC). Stable water isotope composition of the shallow ice core drilled at the GV7 site in 2013-2014. Dating the ice core/Paleoclimate research (https://dx.doi.org/doi:10.22663/KOPRI-KPDC-00000654). Climate Reanalyzer (https://climatereanalyzer.org/) from the Climate Change Institute, University of Maine, US, is publicly available.

Author contributions. YN: Conceptualization, Data analysis, Writing – original draft, Review and editing. YH: Conceptualization, Data analysis, Review and editing. SDH: Conceptualization, Review and editing. HK: Conceptualization, Review and editing. SK: Data analysis, Review and editing, JM: Data analysis, Review and editing, BS: Conceptualization, Review and editing, JL: Conceptualization, Review and editing.

Competing interests. The authors declare that they have no conflict of interest.

Financial support. This work was supported by a Korea Polar Research Institute grant (PE25100) and a National Research Foundation of Korea grant funded by the Korean government (2022R1A2C3007047). This work was partially supported by Korea Institute of Marine Science & Technology Promotion (KIMST) funded by the Ministry of Oceans and Fishers (RS-2023-00256677; PM23020).

References

Becagli, S., Proposito, M., Benassai, S., Flora, O., Genoni, L., Gragnani, R., Largiuni, O., Pili, S.L., Severi, M., Stenni, B., Traversi, R., Udisti, R., and Frezzotti, M.: Chemical and isotopic snow variability in East Antarctica along the 2001/02 ITASE traverse. Annals of Glaciology, 39, 473–482. https://doi.org/10.3189/172756404781814636, 2004.

Beal, L.M., Vialard, J., Roxy, M.K., and lead authors.: IndOOS-2: a roadmap to sustained observations of the Indian Ocean for 2020–2030. CLIVAR-4/2019. https://doi.org/10.36071/clivar.rp.4-1.2019, 2019.

Bertler, N. A. N., Barrett, P. J., Mayewski, P. A., Fogt, R. L., Kreutz, K. J., and Shulmeister, J.: El Ni˜no suppresses Antarctic warming, Geophys. Res. Lett., 31, L15207, doi:10.1029/2004GL020749, 2004.

Bertler, N.A.N, Mayewski, P., and Carter, L.: Cold conditions in Antarctica during the Little Ice Age – implications for abrupt climate change mechanisms. Earth and Planetary Science Letters, 308, 41–51, https://doi.org/10.1016/j.epsl.2011.05.021, 2011.

Bertler, N. A. N., Conway, H., Dahl-Jensen, D., Emanuelsson, D. B., Winstrup, M., Vallelonga, P. T., Lee, J. E., Brook, E. J., Severinghaus, J. P., Fudge, T. J., Keller, E. D., Baisden, W. T., Hindmarsh, R. C. A., Neff, P. D., Blunier, T., Edwards, R., Mayewski, P. A., Kipfstuhl, S., Buizert, C., Canessa, S., Dadic, R., Kjær, H. A., Kurbatov, A., Zhang, D., Waddington, E. D., Baccolo, G., Beers, T., Brightley, H. J., Carter, L., Clemens-Sewall, D., Ciobanu, V. G., Delmonte, B., Eling, L., Ellis, A., Ganesh, S., Golledge, N. R., Haines, S., Handley, M., Hawley, R. L., Hogan, C. M., Johnson, K. M., Korotkikh, E., Lowry, D. P., Mandeno, D., McKay, R. M., Menking, J. A., Naish, T. R., Noerling, C., Ollive, A., Orsi, A., Proemse, B. C., Pyne, A. R., Pyne, R. L., Renwick, J., Scherer, R. P., Semper, S., Simonsen, M., Sneed, S. B., Steig, E. J., Tuohy, A., Venugopal, A. U., Valero-Delgado, F., Venkatesh, J., Wang, F., Wang, S., Winski, D. A., Winton, V. H. L., Whiteford, A., Xiao, C., Yang, J., and Zhang, X.: The Ross Sea dipole – temperature, snow accumulation and sea ice variability in the Ross Sea region, Antarctica, over the past 2700 years. Climate of the Past, 14, 193–214. https://doi.org/10.5194/cp-14-193-2018, 2018.

Caiazzo, L., Baccolo, G., Barbante, C., Becagli, S., Berto, M., Ciardini, V., Crotti, I., Delmonte, B., Dreossi, G., Frezzotti, M., Gabrieli, J., Giardi, F., Han, Y., Hong, S-B., Hur, S.D., Hwang, H., Kang, J-H., Narcisi, B., Proposito, M., Scarchilli, C., Selmo, E., Severi, M., Spolaor, A., Traversi, R., and Udisti, R.: Prominent features in isotopic, chemical and dust stratigraphies from coastal East Antarctic ice sheet (Eastern Wilkes Land). Chemosphere, 176, 273-287. https://doi.org/10.1016/j.chemosphere.2017.02.11, 2017.

Clem, K. R., and Fogt, R. L. Varying roles of ENSO and SAM on the Antarctic Peninsula climate in austral spring. Journal of Geophysical Research: Atmospheres, 118(20), 11,481–11,492. https://doi.org/10.1002/jgrd.50860, 2013.

Cohen, L., S. Dean, and J. Renwick.: Synoptic Weather Types for the Ross Sea Region, Antarctica. J. Climate, 26, 636–649, https://doi.org/10.1175/JCLI-D-11-00690.1, 2012.

Constable, A.J., Harper,S., Dawson, J., Holsman, K., Mustonen, T., Piepenburg, D., and Rost, B.: Cross-Chapter Paper 6: Polar Regions. In: Climate Change 2022: Impacts, Adaptation and Vulnerability. Contribution of Working Group II

to the Sixth Assessment Report of the Intergovernmental Panel on Climate Change [H.-O. Pörtner, D.C. Roberts, M. Tignor,E.S. Poloczanska, K. Mintenbeck, A. Alegría, M. Craig, S. Langsdorf, S. Löschke, V. Möller, A. Okem, B. Rama (eds.)].Cambridge University Press, Cambridge, UK and New York, NY, USA, pp. 2319–2368, doi:10.1017/9781009325844.023, 2022.

Craig, H.: Isotopic variations in meteoric waters. Science, 133, 1702–1703. DOI: 10.1126/science.133.3465.1702, 1961.

Dalaiden, Q., Goosse, H., Lenaerts, J.T.M., Cavitte, M.G.P., and Henderson, N.: Future Antarctic snow accumulation trend is dominated by atmospheric synoptic-scale events. Communications Earth & Environment, 1, 62. https://doi.org/10.1038/s43247-020-00062-x, 2020a.

Dalaiden, Q., Goosse, H., Klein, F., Lenaerts, J. T. M., Holloway, M., Sime, L., and Thomas, E.R.: How useful is snow accumulation in reconstructing surface air temperature in Antarctica? A study combining ice core records and climate models, The Cryosphere, 14, 1187–1207, https://doi.org/10.5194/tc-14-1187-2020, 2020b.

Delmotte, M., Masson, V., Jouzel J, and Morgan, V.: A seasonal deuterium excess signal at Law Dome, coastal Eastern Antarctica: a Southern Ocean signature. Journal of Geophysical Research 105(D6): 7187–7197, 2000.

Ding, Q., Steig, E. J., Battisti, D. S., and Wallace, J. M.: Influence of the tropics on the Southern Annular Mode. Journal of Climate, 25 (18), 6330–6348. https://doi.org/10.1175/JCLI-D-11-00523.1, 2012.

Divine, D. V., E. Isaksson, M. Kaczmarska, F. Godtliebsen, H. Oerter, E. Schlosser, S. J. Johnsen, M. van den Broeke, and R. S. W. van de Wal.: Tropical Pacific–high latitude south Atlantic teleconnections as seen in $\delta^{18}O$ variability in Antarctic coastal ice cores, J. Geophys. Res., 114, D11112, doi:10.1029/2008JD010475, 2009.

Dong, L., Zhou, T., and Wu, B.: Indian Ocean warming during 1958–2004 simulated by a climate system model and its mechanism. Clim Dyn 42, 203–217. https://doi.org/10.1007/s00382-013-1722-z, 2014.

Ejaz, T., Rahaman, W., Laluraj, C.M., Mahalinganathan, K., and Thamban, M.: Rapid Warming Over East Antarctica Since the 1940s Caused by Increasing Influence of El Niño Southern Oscillation and Southern Annular Mode. Front. Earth Sci. 10:799613. doi: 10.3389/feart.2022.799613, 2022.

Fogt, R. L., Wovrosh, A. J., Langen, R. A., and Simmonds, I.: The characteristic variability and connection to the underlying synoptic activity of the Amundsen-Bellingshausen Seas Low. Journal of Geophysical Research, 117, D07111. doi:10.1029/2011JD017337, 2012.

Fogt, R.L., and Marshall GJ.: The Southern Annular Mode: Variability, trends, and climate impacts across the Southern Hemisphere. WIREs Clim Change. 2020; 11:e652. https://doi.org/10.1002/wcc.652, 2020.

Fogt, R. L., Raphael, M. N., and Handcock, M.S.: Seasonal Antarctic Sea Ice Extent Reconstructions, 1905-2020, Version 1. [East Antarctica and Ross-Amundsen reconstruction ensembles]. Boulder, Colorado USA. NSIDC:National Snow and Ice Data Center. https://doi.org/10.7265/55x7-we68, 2023.

Fretwell, P., Pritchard, H. D., Vaughan, D. G., Bamber, J. L., Barrand, N. E., Bell, R., Bianchi, C., Bingham, R. G., Blankenship, D. D., Casassa, G., Catania, G., Callens, D., Conway, H., Cook, A. J., Corr, H. F. J., Damaske, D., Damm, V., Ferraccioli, F., Forsberg, R., Fujita, S., Gim, Y., Gogineni, P., Griggs, J. A., Hindmarsh, R. C. A., Holmlund, P., Holt,

J. W., Jacobel, R. W., Jenkins, A., Jokat, W., Jordan, T., King, E. C., Kohler, J., Krabill, W., Riger-Kusk, M., Langley, K. A., Leitchenkov, G., Leuschen, C., Luyendyk, B. P., Matsuoka, K., Mouginot, J., Nitsche, F. O., Nogi, Y., Nost, O. A., Popov, S. V., Rignot, E., Rippin, D. M., Rivera, A., Roberts, J., Ross, N., Siegert, M. J., Smith, A. M., Steinhage, D., Studinger, M., Sun, B., Tinto, B. K., Welch, B. C., Wilson, D., Young, D. A., Xiangbin, C., and Zirizzotti, A.: Bedmap2: improved ice bed, surface and thickness datasets for Antarctica, The Cryosphere, 7, 375–393, https://doi.org/10.5194/tc-7-375-2013.

Frezzotti, M., Urbini, S., Proposito, M., Scarchilli, C., and Gandolfi, S.: Spatial and temporal variability of surface mass balance near Talos Dome, East Antarctica. Journal of Geophysical Research, 112, F02032. https://doi.org/10.1029/2006JF000638, 2007.

Frieler, K., Clark, P., He, F., Buizert, C., Reese, R., Ligtenberg, S.R.M., van den Broeke, M.R., Winkelmann, R., and Levermann, A.: Consistent evidence of increasing Antarctic accumulation with warming. Nature Climate Change, 5, 348–352. https://doi.org/10.1038/nclimate2574, 2015.

Goursaud, S., Masson-Delmotte, V., Favier, V., Preunkert, S., Fily, M., Gallée, H., Jourdain, B., Legrand, M., Magand, O., Minster, B., and Werner, M.: A 60-year ice-core record of regional climate from Adélie Land, coastal Antarctica. The Cryosphere, 11, 343–362. doi: 10.5194/tc-11-343-2017, 2017.

Goursaud, S., Masson-Delmotte, V., Favier, V., Preunkert, S., Legrand, M., Minster, B., and Werner, M.: Challenges associated with the climatic interpretation of water stable isotope records from a highly resolved firn core from Adélie Land, coastal Antarctica. The Cryosphere, 13, 1297–1324. https://doi.org/10.5194/tc-13-1297-2019, 2019.

Hall, A., and Visbeck, M.: Synchronous variability in the southern hemisphere atmosphere, sea ice, and ocean resulting from the annular mode. Journal of Climate, 15: 3043–3057. https://doi.org/10.1175/1520-0442(2002)015<3043:SVITSH>2.0.CO;2, 2002.

Huang, B., Thorne, P.W., Banzon, V.F., Boyer, T., Chepurin, G., Lawrimore, J.H., Menne, M.J., Smith, T.M., Vose, R.S., and Zhang, H-M.: NOAA Extended Reconstructed Sea Surface Temperature (ERSST), Version 5. [Southern Hemisphere Ocean Temperature Anomalies]. NOAA National Centers for Environmental Information. doi:10.7289/V5T72FNM, 2017.

Ionita, M., Scholz, P., Grosfeld, K., and Treffeisen, R.: Moisture transport and Antarctic sea ice: austral spring 2016 event, Earth Syst. Dynam., 9, 939–954, https://doi.org/10.5194/esd-9-939-2018, 2018.

IPCC, 2001: Climate Change 2001: The Scientific Basis. Contribution of Working Group I to the Third Assessment Report of the Intergovernmental Panel on Climate Change [Houghton, J.T.,Y. Ding, D.J. Griggs, M. Noguer, P.J. van der Linden, X. Dai, K. Maskell, and C.A. Johnson (eds.)]. Cambridge University Press, Cambridge, United Kingdom and New York, NY, USA, 881pp.

IPCC, 2019: Technical Summary [H.-O. Pörtner, D.C. Roberts, V. Masson-Delmotte, P. Zhai, E. Poloczanska, K. Mintenbeck, M. Tignor, A. Alegría, M. Nicolai, A. Okem, J. Petzold, B. Rama, N.M. Weyer (eds.)]. In: IPCC Special Report on the Ocean and Cryosphere in a Changing Climate [H.- O. Pörtner, D.C. Roberts, V. Masson-Delmotte, P. Zhai, M.

Tignor, E. Poloczanska, K. Mintenbeck, A. Alegría, M. Nicolai, A. Okem, J. Petzold, B. Rama, N.M. Weyer (eds.)]. In press.

Jackson, S. L., Vance, T. R., Crockart, C., Moy, A., Plummer, C., and Abram, N. J.: Climatology of the Mount Brown South ice core site in East Antarctica: implications for the interpretation of a water isotope record. Climate of the Past, 19, 1653–1675. https://doi.org/10.5194/cp-19-1653-2023, 2023.

Jouzel, J., Merlivat, L., and Lorius, C.: Deuterium excess in an East Antarctic ice core suggests higher relative humidity at the oceanic surface during the last glacial maximum. Nature, 299, 688–691. https://doi.org/10.1038/299688a0S, 1982.

Jouzel, J., Alley, R. B., Cuffey, K. M., Dansgaard, W., Grootes, P., Hoffmann, G., Johnsen, S.J., Koster, R.D., Peel, D., Shuman, C.A., Stievenard, M., Stuiver, M., and White, J.: Validity of the temperature reconstruction from water isotopes in ice cores. Journal of Geophysical Research Oceans, 102, 26471–26487, https://doi.org/10.1029/97JC01283, 1997.

Khan. I. (2019). Climate-related variability of isotopic records in a coastal Antarctic ice (Master's thesis). Retrieved from [http://hdl.handle.net/10579/15637]. Venice, Italy: Università Ca' Foscari Venezia.

Kim, BH., Seo, KW., Eom, J., Chen, J., and Wilson., C.: Antarctic ice mass variations from 1979 to 2017 driven by anomalous precipitation accumulation. Scientific Reports, 10, 20366. https://doi.org/10.1038/s41598-020-77403-5, 2020.

Kim, J., Kang, D., Lee, M.-I., Jin, E. K., Kug, J.-S., and Lee, W. S. (2023). Remote influences of ENSO and IOD on the interannual variability of the West Antarctic sea ice. Journal of Geophysical Research: Atmospheres, 128, e2022JD038313. https://doi.org/10.1029/2022JD038313

Kino, K., Okazaki, A., Cauquoin, A., and Yoshimura, K.: Contribution of the Southern Annular Mode to variations in water isotopes of daily precipitation at Dome Fuji, East Antarctica. Journal of Geophysical Research: Atmospheres, 126, e2021JD035397. https://doi. org/10.1029/2021JD035397, 2021.

Klein, F., Abram, N. J., Curran, M. A. J., Goosse, H., Goursaud, S., Masson-Delmotte, V., Moy, A., Neukom, R., Orsi, A., Sjolte, J., Steiger, N., Stenni, B., and Werner, M.: Assessing the robustness of Antarctic temperature reconstructions over the past 2 millennia using pseudoproxy and data assimilation experiments, Climate of Past, 15, 661–684. https://doi.org/10.5194/cp-15-661-2019, 2019.

Lee, H-J., and Jin, E.M.: The dominant influence of indian ocean dipole-like ocean warming on decreased precipitation over eastern East Antarctica. Front. Earth Sci. 12:1387809. doi: 10.3389/feart.2024.1387809, 2024.

Leroy-Dos Santos, C., Fourré, E., Agosta, C., Casado, M., Cauquoin, A., Werner, M., Minster, B., Prié, F., Jossoud, O., Petit, L., and Landais, A.: From atmospheric water isotopes measurement to firn core interpretation in Adélie Land: a case study for isotope-enabled atmospheric models in Antarctica. The Cryosphere, 17, 5241–5254. https://doi.org/10.5194/tc-17-5241-2023, 2023.

Lewis, S.C., LeGrande, A.N., Kelley, M., and Schmidt, G.A.: Modeling insights into deuterium excess as an indicator of water vapor source conditions. J. Geophys. Res. Atmos., 118, no. 2, 243-262, doi:10.1029/2012JD017804, 2013.

Liu H., Jezek K.C., Li B. and Zhao Z.: Radarsat Antarctic Mapping Project Digital Elevation Model, Version 2. Boulder, Colorado USA. NASA National Snow and Ice Data Center Distributed Active Archive Center. doi: 10.5067/8JKNEW6BFRVD, 2015.

Magand, O., Frezzotti, M., Pourchet, M., Stenni,B., Genoni, L., and Fily, M.: Climate variability along latitudinal and longitudinal transects in east Antarctica. Annals of Glaciology, 39, 351–358. doi:10.3189/172756404781813961, 2004.

Markle, B. R., and Steig, E. J.: Improving temperature reconstructions from ice-core water-isotope records. Climate of the Past, 18, 1321–1368. https://doi.org/10.5194/cp-18-1321-2022, 2022.

Masson-Delmotte, V., Delmotte, M., Morgan, V., Etheridge, D., van Ommen, T., Tartarin, S., and Hoffmann, G.: Recent southern Indian Ocean climate variability inferred from a Law Dome ice core: new insights for the interpretation of coastal Antarctic isotopic records. Climate Dynamics 21, 153–166. https://doi.org/10.1007/s00382-003-0321-9, 2003.

Masson-Delmotte, V. S., Hou, S., Ekaykin, A., Jouzel, J., Aristarain, A., Bernardo, R.T., Bromwich, D., Cattani, O., Delmotte, M., Falourd, S., Frezzotti, M., Gallée, H., Genoni, L., Isaksson, E., Landais, A., Helsen, M.M., Hoffmann, G., Lopez, J., Morgan, V., Motoyama, H., Noone, D., Oerter, H., Petit, J.R., Royer, A., Uemura, R., Schmidt, G.A., Schlosser, E., Simões, J.C., Steig, E.J., Stenni, B., Stievenard, M., van den Broeke, M.R., van de Wal, R.S.W., van de Berg, W.J., Vimeux, F., and White, J.W.C.: A review of Antarctic surface snow isotopic composition: Observations, atmospheric circulation, and isotopic modeling. Journal of Climate, 21, 3359-3387. doi:10.1175/2007JCLI2139.1, 2008.

Matsuoka, K., Skoglund, A., Roth, G., de Pomereu, J., Griffiths, H., and Headland, R.: Quantarctica, an integrated mapping environment for Antarctica, the Southern Ocean, and sub-Antarctic islands. Environmental Modelling & Software 140, 105015. doi:10.1016/j.envsoft.2021.105015, 2021.

Mayewski, P. A., Meredith, M.P., Summerhayes, C.P., Turner, J., Worby, A., Barrett, J., Casassa, G., Bertler, N.A.N., Bracegirdle, A.C., Garabato, N., Bromwich, D., Campbell, H., Hamilton, G.S., Lyons, W.B., Maasch, K.A., Aoki, S., Xiao, C., and Tas van Ommen.: State of the Antarctic and Southern Ocean climate system, Rev. Geophys., 47, RG1003, doi:10.1029/2007RG000231, 2009.

Medley, B., McConnell, J. R., Neumann, T. A., Reijmer, C. H., Chellman, N., Sigl, M., and Kipfstuhl, S.: Temperature and Snowfall in Western Queen Maud Land Increasing Faster Than Climate Model Projections. Geophysical Research Letter, 45, 1472–1480. https://doi.org/10.1002/2017GL075992, 2018.

Meyerson, E.A., Mayewski, P.A., Kreutz, K.J., David Meeker, L., Whitlow, S.I, and Twickler, M.S.: The polar expression of ENSO and sea-ice variability as recorded in a South Pole ice core. Annals of Glaciology, 2002;35:430-436. doi:10.3189/172756402781817149, 2002.

Nardin, R., Severi, M., Amore, A., Becagli, S., Burgay, F., Caiazzo, L., Ciardini, V., Dreossi, G., Frezzotti, M., Hong, S.-B., Khan, I., Narcisi, B. M., Proposito, M., Scarchilli, C., Selmo, E., Spolaor, A., Stenni, B., and Traversi, R.: Dating of

the GV7 East Antarctic ice core by high-resolution chemical records and focus on the accumulation rate variability in the last millennium. Climate of the Past, 17, 2073–2089, https://doi.org/10.5194/cp-17-2073-2021, 2021.

Nicolas, J. P., and Bromwich, D. H.: New Reconstruction of Antarctic Near-Surface Temperatures: Multidecadal Trends and Reliability of Global Reanalyses, Journal of Climate, 27(21), 8070-8093. https://doi.org/10.1175/JCLI-D-13-00733.1, 2014.

Nyamgerel, Y., Han, Y., Kim, S., Hong, S., Lee, J., and Hur, S. Chronological characteristics for snow accumulation on Styx Glacier in northern Victoria Land, Antarctica. Journal of Glaciology, 66(260), 916-926. doi:10.1017/jog.2020.53, 2020.

Nyamgerel, Y., Han, Y., Hwang, H., Han, C., Hong, S., Hur, S., and Lee, J.: Climate-related variabilities in the Styx-M ice core record from northern Victoria Land, East Antarctica, during 1979–2014, Science of The Total Environment, 935, 173319, doi.org/10.1016/j.scitotenv.2024.173319, 2024.

Oerter, H., Wilhelms, F., Jung-Rothenhausler, F., Goktas, F., Miller, H., Graf, W., and Sommer, S.: Accumulation rates in Dronning Maud Land, Antarctica, as revealed by dielectric-profiling measurements of shallow firn cores. Annals of Glaciology, 30, 27–34, https://doi.org/10.3189/172756400781820705, 2000.

Palerme, C., Genthon, C., Claud, C., Kay, J.E., Wood, N.B., and L'Ecuyer, T.: Evaluation of current and projected Antarctic precipitation in CMIP5 models. Climate Dynamics, 48, 225–239. https://doi.org/10.1007/s00382-016-3071-1, 2017.

Pohl, B., Favier, V., Wille, J., Udy, D. G, Vance, T. R, Pergaud, J., Dutrievoz, N., Blanchet, J., Kittel, C., Amory, C., Krinner, G., Codron, F.: Relationship between weather regimes and atmospheric rivers in East Antarctica. Journal of Geophysical Research: Atmospheres, 126, e2021JD035294. https://doi.org/10.1029/2021JD035294, 2021.

Purich, A., England, M. H., Cai, W., Chikamoto, Y., Timmermann, A., Fyfe, J. C., Frankcombe, L., Meehl, G.A., and Arblaster, J.M.: Tropical Pacific SST Drivers of Recent Antarctic Sea Ice Trends. Journal of Climate, 29(24), 8931-8948, https://doi.org/10.1175/JCLI-D-16-0440.1, 2016.

Rignot, E., Mouginot, J., Scheuchl, B., van den Broeke, M., van Wessem, M. J., and Morlighem, M.: Four decades of Antarctic Ice Sheet mass balance from 1979-2017. Proceedings of the National Academy of Sciences of the United States of America, 116(4), 1095–1103. https://doi.org/10.1073/pnas.1812883116, 2019.

Rintoul, S.R., Chown, S.L., DeConto, R.M., England, M.H., Fricker, H.A., Masson-Delmotte, V., Naish, T.R., Sieger, M.J., and Xavier, J.C.: Choosing the future of Antarctica. Nature 558, 233–241 (2018). https://doi.org/10.1038/s41586-018-0173-4, 2018.

Roberts, J., Plummer, C., Vance, T., van Ommen, T., Moy, A., and Poynter, S.: A 2000 year annual record of snow accumulation rates for Law Dome, East Antarctica. Climate of the Past, 11 (5). pp. 69770. https://doi.org/10.5194/cp116972015, 2015.

Russell, A., and McGregor, G.R.: Southern hemisphere atmospheric circulation: impacts on Antarctic climate and reconstructions from Antarctic ice core data. Climatic Change, 99, 155–192. https://doi.org/10.1007/s10584-009-9673-4, 2010, 2010.

Schneider, D. P., and Steig, E. J.: Ice cores record significant 1940s Antarctic warmth related to tropical climate variability. Proc. Natl. Acad. Sci. U.S.A. 105, 12154–12158, 2008.

Schlosser, E., and Oerter, H.: Seasonal variations of accumulation and the isotope record in ice cores: a study with surface snow samples and firn cores from Neumayer station, Antarctica. Annals of Glaciology. 2002;35:97-101. doi:10.3189/172756402781817374, 2002.

Schlosser, E., H. Anschütz, D. Divine, T. Martma, A. Sinisalo, S. Altnau, and E. Isaksson.: Recent climate tendencies on an East Antarctic ice shelf inferred from a shallow firn core network, J. Geophys. Res. Atmos., 119, 6549–6562, doi:10.1002/2013JD020818, 2014.

Sodemann, H., and Stohl, A.: Asymmetries in the moisture origin of Antarctic precipitation. Geophysical Research Letters, 36, L22803, doi:10.1029/2009GL040242, 2009.

Servettaz, A. P. M., Orsi, A. J., Curran, M. A. J., Moy, A. D., Landais, A., Agosta, C., Holly, V., Winton, L., Touzeau, A., McConnell, J.R., Werner, M., and Baroni, M.: Snowfall and water stable isotope variability in East Antarctica controlled by warm synoptic events. Journal of Geophysical Research Atmospheres, 125, e2020JD032863. https://doi.org/10.1029/2020JD032863, 2020.

Sharma, S., Ha, KJ., Yamaguchi, R., Rodgers, K.B., Timmermann, A., and Chung, E-S.: Future Indian Ocean warming patterns. Nat Commun 14, 1789 (2023). https://doi.org/10.1038/s41467-023-37435-7, 2023.

Simmonds, I., Keay, K., Lim, E-P.: Synoptic activity in the seas around Antarctica. Mon. Wea. Rev., 131, 272–288, https://doi.org/ 10.1175/1520-0493(2003)131,0272:SAITSA.2.0.CO;2.

Stenni, B., Caprioli, R., Cimino, L., Cremisini, C., Flora, O., Gragnani, R., Longinelli, A., Maggi, V., and Torcini, S.: Years of isotope and chemical records in a firn core from Hercules Névé, Northern Victoria Land, Antarctica. Annals of Glaciology, 29, 106–112. doi: 10.3189/172756499781821175, 1999.

Stenni, B., Masson-Delmotte, V., Johnsen, S., Jouzel, J., Longinelli, A., Monnin, E., Rothlisberger, R., and Selmo, E.: An oceanic cold reversal during the last deglaciation. Science. 2001 Sep 14;293(5537):2074-7. doi: 10.1126/science.1059702. PMID: 11557889, 2001.

Stenni, B., Proposito, M., Gragnani., R., Flora, O., Jouzel, J., Falourd, S., and Frezzotti, M.: Eight centuries of volcanic signal and climate change at Talos Dome (East Antarctica). Journal of Geophysical Research, 107(D9), 1–14. doi:10.1029/2000JD000317, 2002.

Stenni, B., Curran, M. A. J., Abram, N. J., Orsi, A., Goursaud, S., Masson-Delmotte, V., Neukom, R., Goosse, H., Divine, D., van Ommen, T., Steig, E. J., Dixon, D. A., Thomas, E. R., Bertler, N. A. N., Isaksson, E., Ekaykin, A., Werner, M., and Frezzotti, M.: Antarctic climate variability on regional and continental scales over the last 2000 years. Climate of the Past, 13, 1609–1634, https://doi.org/10.5194/cp-13-1609-2017, 2017.

Thomas, E. R., Marshall, G. J., and McConnell, J. R.: A doubling in snow accumulation in the western Antarctic Peninsula since 1850. Geophysical Research Letters, 35, L01706, doi:10.1029/2007GL032529, 2008.

Thomas, E. R., and Abram, N. J.: Ice core reconstruction of sea ice change in the Amundsen-Ross Seas since 1702 A.D. Geophysical Research Letters, 43, 5309–5317, doi:10.1002/2016GL068130, 2016.

Thompson, D. and Solomon, S.: Interpretation of recent southern hemisphere climate change, Science, 296(5569), 895-899, 2002.

Timmermann, R., and Hellmer, H. H.: Southern Ocean warming and increased ice shelf basal melting in the twenty-first and twenty-second centuries based on coupled ice-ocean finite-element modelling. Ocean Dynamics, 63(9–10), 1011–1026. https://doi.org/10.1007/s10236-013-0642-0, 2013.

Tuohy, A., Bertler, N., Neff, P., Edwards, R., Emanuelsson, D., Beers, T., and Mayewski, P.: Transport and deposition of heavy metals in the Ross Sea Region, Antarctica, Journal of Geophysical. Research. Atmospheres, 120, 10,996– 11,011. doi:10.1002/2015JD023293, 2015.

Turner, J., R.A., Bindschadler, P., Convey, G., di Prisco, E., Fahrbach, J., Gutt, D.A., and Hodgson, P.A.: Mayewski and C.P. Summerhayes (editors). (2009). Antarctic climate change and the environment. Cambridge: Scientific Committee on Antarctic Research.

Turner, J., Phillips, T., Thamban, M., Rahaman, W., Marshall, G. J., Wille, J. D., Favier, V., Winton, V.H.L., Thomas, E., Wang, Z., van den Broeke, M., Hosking, J.S., and Lachlan-Cope, T.: The dominant role of extreme precipitation events in Antarctic snowfall variability. Geophysical Research Letters, 46, 3502–3511. https://doi.org/10.1029/2018GL081517, 2019.

Udy, D. G., T. R. Vance, A. S. Kiem, N. J. Holbrook, and M. A. J. Curran.: Links between Large-Scale Modes of Climate Variability and Synoptic Weather Patterns in the Southern Indian Ocean. J. Climate, 34, 883–899, https://doi.org/10.1175/JCLI-D-20-0297.1, 2021.

Uemura, R., Matsui, Y., Yoshimura, K., Motoyama, H., and Yoshida., N.: Evidence of deuterium excess in water vapor as an indicator of ocean surface conditions, J. Geophys. Res., 113, D19114, doi:10.1029/2008JD010209, 2008.

Vance, T. R., Roberts, J. L., Moy, A. D., Curran, M. A. J., Tozer, C. R., Gallant, A. J. E., Abram, N. J., van Ommen, T. D., Young, D. A., Grima, C., Blankenship, D. D., and Siegert, M. J.: Optimal site selection for a high-resolution ice core record in East Antarctica, Climate of the Past, 12(3): 595-610, 2016.

Wille, J. D., Favier, V., Gorodetskaya, I. V., Agosta, C., Kittel, C., Beeman, J. C., Jourdian, N.C., Lenaerts, J.T.M., Codron, F.: Antarctic atmospheric river climatology and precipitation impacts. Journal of Geophysical Research: Atmospheres, 126, e2020JD033788. https://doi. org/10.1029/2020JD033788, 2021.

Yuan, X.: ENSO-related impacts on Antarctic sea ice: a synthesis of phenomenon and mechanisms. Antarctic Science. 2004;16(4):415-425. doi:10.1017/S0954102004002238, 2004.

Zhang, P. and Duan, A.: Connection between the Tropical Pacific and Indian Ocean and Temperature Anomaly across West Antarctic. npj Clim Atmos Sci 6, 49. https://doi.org/10.1038/s41612-023-00381-8, 2023.

Zhang, L., Ren, X., Cai, W., Li, X., and Wu, L.: Weakened western Indian Ocean dominance on Antarctic sea ice variability in a changing climate. Nat Commun 15, 3261 (2024). https://doi.org/10.1038/s41467-024-47655-0, 2024.